foods

MDPI

Article

Traditional Vinegar Processing Enhances the Bile Acid-Modulating Effects of Qingpi (Citri Reticulatae Pericarpium Viride): Insights from Chemical Profiling and Metabolomics

Qian Zhang, Mingxuan Li, Rong Xue, Xi Mei, Lianlin Su, Jinguo Xu, Chunqin Mao, Guojun Yan *,† and Tulin Lu *,†

College of Pharmacy, Nanjing University of Chinese Medicine, Nanjing 210023, China

* Correspondence: yanguojun@njucm.edu.cn (G.Y.); ltl2021@njucm.edu.cn (T.L.)

† These authors contributed equally to this work.

Abstract

Qingpi, the dried young fruit of Citrus species, has been consumed in China for over a thousand years as both a culinary ingredient and a traditional food-medicine substance, yet the chemical basis underlying its food-related health properties and the effect of traditional vinegar processing remain poorly characterized. This study integrated LC-MS/MS chemical profiling with an ANIT-induced cholestatic rat model to examine how vinegar processing alters the chemical profile of Qingpi and how this relates to its bile acid-modulating potential as a food ingredient. A total of 52 components were characterized, of which 9 were confirmed with authentic reference standards. A total of 10 differential components revealed that the chemical changes induced by vinegar processing predominantly occurred in the flavonoid class. In the rat model, Qingpi intervention improved bile flow and liver histopathology. Untargeted metabolomics identified primary bile acid biosynthesis as the most significantly enriched pathway, and targeted bile acid metabolomics further revealed that Qingpi modulated the serum bile acid profile, with the vinegar-processed form showing stronger regulatory effects than the raw form. Mechanistically, Qingpi restored the expression of hepatic FXR, BSEP, and MRP2 and downregulated CYP7A1, as validated by RT-qPCR and Western blotting, indicating an association with the FXR signaling pathway. Furthermore, vinegar processing enhanced these expression changes, which corresponded to its stronger modulatory effect on the serum bile acid profile. These findings characterize the chemical basis of Qingpi as a traditional edible plant and support vinegar processing as a traditional food-processing strategy that alters its functional phytochemical profile and enhances its bile acid-modulating potential.

Keywords: Qingpi; vinegar processing; flavonoid profile; bile acid metabolism; FXR signaling pathway

Academic Editor: Marina Russo

Received: 27 October 2026
Revised: 24 November 2026
Accepted: 25 November 2026
Published: 29 November 2026

Copyright: © 2026 by the authors. Licensee MDPI, Basel, Switzerland. This article is an open access article distributed under the terms and conditions of the Creative Commons Attribution (CC BY) license.

1. Introduction

Cholestatic liver disease (CLD) refers to a group of hepatobiliary disorders characterized by impaired formation, secretion, and excretion of bile. Persistent impairment of bile flow leads to intrahepatic accumulation of bile acids and progressive hepatocellular

injury, which can advance to hepatic fibrosis, cirrhosis, and liver failure [1]. Currently, pharmacological options remain limited and highly disease-specific. While ursodeoxycholic acid (UDCA) is the standard first-line therapy for primary biliary cholangitis (with elafibranor and seladelpar recently approved under accelerated approval for specific subgroups), a substantial proportion of patients still exhibit inadequate response [2,3]. Moreover, for other forms of CLD, such as primary sclerosing cholangitis (PSC), no effective pharmacological therapy has been approved to date. These limitations have motivated growing interest in dietary and food-derived ingredients that may modulate bile acid metabolism and reduce the risk of cholestatic progression.

In recent years, natural food-derived products have attracted increasing attention as dietary interventions relevant to CLD, owing to their multi-target effects and favorable safety profiles [4]. Qingpi (Citri reticulatae pericarpium viride) stands out as a promising candidate. Derived from the young fruit of citrus species, Qingpi has been consumed in culinary and medicinal contexts in China for over a thousand years [5]. It has a long history of use as both a culinary ingredient and a traditional food-derived material to support liver health, with its raw and processed forms being well-documented in traditional dietary practices [6,7]. Phytochemical investigations have identified flavonoids as one of the principal bioactive constituent classes of Qingpi [8,9]. These compounds have been reported to exhibit a range of bioactivities, including anti-oxidant and anti-inflammatory properties, effects on glycolipid metabolism, and hepatoprotective and choleretic activities, with hesperidin, neohesperidin, and naringenin among the representative flavonoids [10,11]. Vinegar processing, a traditional practice applied to Qingpi, is known to alter its constituent profile, yet how such processing affects the chemical basis of these health effects remains poorly characterized [12].

Choleretic activity and effects on bile acid have been reported for Qingpi and its flavonoid constituents in particular [13,14]. Given that bile acid accumulation is a central feature of cholestasis, bile acid homeostasis provides a mechanistic link between Qingpi's chemical profile and its health-related effects. Under physiological conditions, the composition and proportion of bile acids remain tightly regulated. However, when bile acid metabolism is disrupted, excessive accumulation of toxic bile acids occurs, triggering hepatocyte apoptosis, inflammation, and progressive liver damage, which may ultimately culminate in cirrhosis and liver failure [15]. The farnesoid X receptor (FXR) is a master regulator of bile acid homeostasis. Activation of FXR indirectly suppresses bile acid synthesis by downregulating the expression of cholesterol 7α-hydroxylase (CYP7A1), the rate-limiting enzyme in the classic bile acid synthesis pathway. Concurrently, FXR promotes bile acid efflux from hepatocytes into the biliary tract by upregulating transporters such as the bile salt export pump (BSEP) and multidrug resistance-associated protein 2 (MRP2) [16–18]. Thus, bile acid metabolism and the FXR signaling pathway provide a mechanistic framework for evaluating the health-related effects of Qingpi and for examining whether traditional processing modifies these effects.

Against this background, this study characterized the chemical profiles of raw and vinegar-processed Qingpi and examined how vinegar processing alters its chemical composition and bile acid-modulating potential, using integrated chemical profiling, serum and bile acid metabolomics, and FXR-pathway analysis in an ANIT-induced cholestatic rat model. This work aims to clarify how processing-induced compositional changes relate to the bile acid-regulating effects of Qingpi and to provide a basis for its use as a functional food ingredient.

2. Materials and Methods

2.1. Chemicals and Materials

Qingpi fruits were purchased from Sanjiu (Shenzhen, China). Raw and vinegar-processed Qingpi slices were prepared as previously reported [11]. All Qingpi fruits were sliced in 3 mm thickness directly and oven dried (50 °C, 3 h) to get R-QP. One half of R-QP was incubated with vinegar (per 100 kg samples with vinegar 15 kg, percentile of vinegar was 15% approximately) and then dried by stir-firing to obtain V-QP, which would be with deeper surface color and a slight vinegar aroma. The vinegar used for processing was Hengshun Zhenjiang Xiangcu (a traditional solid-state fermented Chinese aromatic vinegar, produced by Jiangsu Hengshun Vinegar-Industry Co., Ltd., Jiangsu, China; Batch No. 20200301), with a total acid content of ≥5.5 g·100 mL^{-1}. The processing procedures were conducted in three independent batches to ensure reproducibility. All reference substances used in the study, including hesperidin (Lot: 110721-202019), neohesperidin (Lot:111857-201703), quercetin (Lot: 10081-9905), limonin (Lot: 110800), synephrine (Lot: 110727-202110) and naringin (Lot: 110722-201815) were purchased from National Institutes for Food and Drug Control (Beijing, China). Nobiletin (Lot: 130108) was from WeiKeQi (Chengdu, China). Narirutin (Lot:201902) was purchased from SenBeiJia (Nanjing, China). Rutin (Lot: Y22S653719) was purchased from Yuanye (Shanghai, China). The purities of the components were all ≥98%. 47 kinds of bile acid methanol mixed standard (Lot: MJ20230601035) were provided from Major (Shanghai, China).

Alpha-naphthyl isothiocyanate (ANIT, Lot: 2224366) and Ursodeoxycholic acid (UDCA, Lot: 2116648) were purchased from Aladdin (Shanghai, China). The antibodies recognizing Glyceraldehyde-3-phosphate dehydrogenase (GAPDH, Lot: YM3029), CYP7A1 (Lot: YM1026), and BSEP, (Lot: YN0507) were provided by Immunoway (Beijing, China). FXR (Lot: AF04768) and MRP2 (Lot: AF02808) were provided by Anpu (Shanghai, China).

2.2. Qingpi Extract Preparation

Both raw and vinegar-processed Qingpi slices were first reflux-extracted twice with 10-fold volumes of 80% ethanol and subsequently with 10-fold volumes of water, each for 1.5 h. The filtrates were combined and concentrated under reduced pressure at 60 °C to a concentration of 0.2 g·mL^{-1} (equivalent to crude Qingpi) for subsequent animal administration and analysis. The three independent processing batches described in Section 2.1 were used for extraction. The mean extraction yields of the final dried extracts across the independent batches were 28.8% (*w*/*w*) for R-QP and 30.2% (*w*/*w*) for V-QP relative to the raw materials.

2.3. Animal Experiments and Treatment

Male SD rats were obtained under license SCXK (Zhejiang) 20190002 and housed under SPF conditions at 25 °C and 40% humidity. After an initial one-week adaptation period, all rats were randomly divided into seven groups (n = 6 per group) using a random-number table: control group (Control), ANIT-model group (Model), ANIT + UDCA group (100 mg kg^{-1}, UDCA), two ANIT + raw-Qingpi groups (0.3 g·kg^{-1}, LR-QP; 0.9 g·kg^{-1}, HR-QP), and two ANIT + vinegar-processed-Qingpi groups (0.3 g·kg^{-1}, LV-QP; 0.9 g·kg^{-1}, HV-QP). From day 1 to day 7, rats in the Control and Model groups received an equal volume of saline by gavage once daily, and rats in the treatment groups received the corresponding Qingpi extract or UDCA by the same route. On day 5, rats in all groups except the Control group received ANIT solution (65 mg·kg^{-1}) by gavage, while the Control group received an equal volume of vehicle. ANIT was dissolved in edible oil and UDCA powder in 0.5% CMC-Na solution; both solutions were shaken to mix and prepared immediately before use. Rats received the corresponding interventions as

scheduled (Figure 1A). On day 7, all rats were anesthetized by intraperitoneal injection of urethane solution (20%, prepared by dissolving urethane powder in normal saline immediately before use) and bile, blood, and liver samples were collected. Following centrifugation at 1000× *g* for 15 min, the separated serum was stored at −80 °C prior to subsequent analysis. For molecular analyses (RT-qPCR and Western blotting), liver samples were taken from the same animals used for the general outcome measurements; three rats per group were randomly selected from the six animals in each group, and each sample represents an independent animal. Investigators performing the biochemical assays and histopathological scoring were blinded to group allocation. The experimental protocol followed the guidelines for the care and use of laboratory animals, and was approved by the Animal Experiment Ethics Committee of Nanjing University of Chinese Medicine (Approval No.:202105A052).

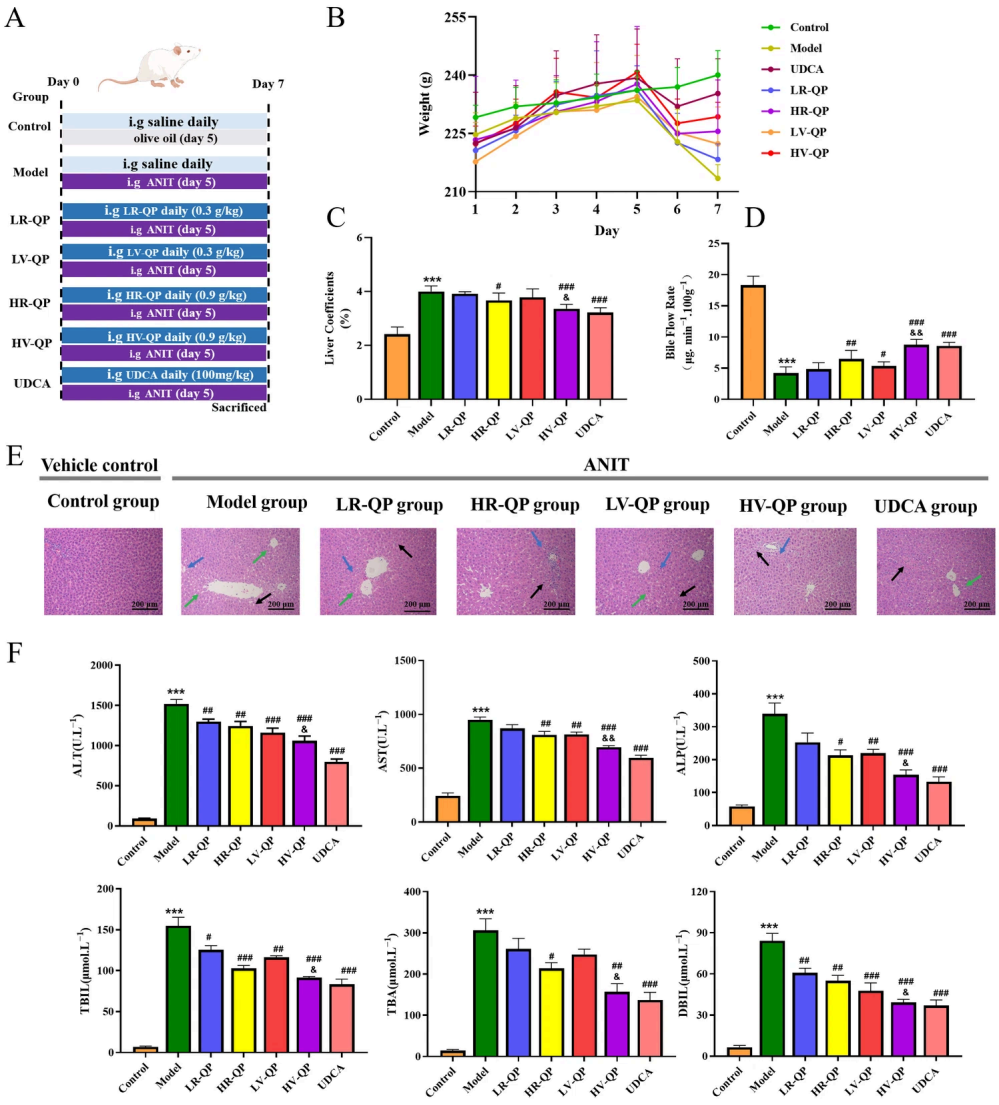


Figure 1. ANIT-induced CLD rat model and the effect of Qingpi intervention. (**A**) Schematic diagram of the animal experimental design. (**B**) Changes in body weight. (**C**) Liver coefficients. (**D**) Bile volume flow. (**E**) Representative H&E staining images of liver tissues (magnification ×400; scale bar = 200 μm; blue arrow: steatosis; black arrow: necrosis; green arrow: eosinophilic bodies). (**F**) Serum levels of ALT, AST, ALP, TBA, TBIL, and DBIL. Data are expressed as mean ± SD (n = 6). *** $p < 0.001$ vs. Control group; # $p < 0.05$, ## $p < 0.01$, ### $p < 0.001$ vs. Model group; & $p < 0.05$, &&

$p < 0.01$ vs. HR-QP group.

2.4. Bile Volume Flow

The operation of bile collection was as follows [19,20]. After anesthetizing the rats for 10 min, the abdominal cavity was quickly opened, the supine position was fixed, the common bile duct intubation and drainage were performed, and the abdomen was covered with normal saline gauze. After successful intubation, rat bile was collected within 30 min, the time and bile weight were recorded, and stored in a −80 °C freezer, and the bile volume flow was represented by the ratio of bile collection to outflow time and rat body weight.

2.5. Biochemical Indicators

The serum function indicators were determined through the application of a colorimetric methodology. Assay kits were purchased from Qiangsheng (Zhejiang, China), including those for: Alanine aminotransferase (ALT, Lot: KH1001-1), aspartate aminotransferase (AST, Lot: KH1002-1), total bile acid (TBA, Lot:KH1009-1), direct bilirubin (DBIL, Lot:KH1005-1), total bilirubin (TBIL, Lot:KH1005-1) and alkaline phosphatase (ALP).

2.6. Body Weight and Organ Coefficient

Body weight of all rats was recorded daily throughout the trial. Physiological states, including urine, coat color, and mental status, were also monitored daily. After blood collection, whole livers were excised, blotted, weighed, and used to calculate the liver coefficient.

2.7. Histopathological Evaluation

A portion of the liver tissues were fixed in 4% paraformaldehyde, embedded in paraffin, and sectioned. Then, the liver sections were stained with hematoxylin and eosin and observed the morphology of the liver tissue by Vectra 3.0 Automated Quantitative Pathology Imaging System (PerkinElmer, Waltham, MA, USA). For each group, sections from three randomly selected rats were examined. The morphology of the liver tissue was assessed at ×400, and representative images were selected to illustrate the predominant histopathological features of each group.

2.8. Qingpi Composition Lc-Ms/ms Analysis

Sample preparations were prepared as follows. The extracts of Qingpi in "2.2" was centrifuged at 4 °C (15,000× *g* for 5 min). A 1.0 mL supernatant aliquot was loaded onto a pre-activated SPE column and subjected to methanol gradient elution (5%, 25%, 50%, 100%). Elution was performed with 1.0 mL of 5% methanol and 2.0 mL methanol for each other gradient. The combined eluates were centrifuged under identical conditions and supernatants were filtered through 0.22 μm filters for analysis. The liquid chromatographic and mass spectrometric conditions were consistent with reported in our previous study [11].

2.9. Serum Metabolomics

Serum samples and LC–MS conditions for metabolomics analysis were prepared following before [11,21]. Mass spectrometry data from each group (Control, Model, UDCA, HR-QP, and HV-QP) were processed using the One-MAP cloud platform to screen differential metabolites. These metabolites were putatively annotated by comparison of their accurate masses and MS/MS spectra with reference spectra from the HMDB, METLIN, and other compound databases, as well as published literature. Metabolic

pathway enrichment analysis of the identified differential metabolites was performed using MetaboAnalyst 6.0 [22,23].

2.10. Bile Acid Targeted Metabolomics

For sample preparation: 100 μL of serum was mixed with 400 μL methanol (containing internal standard), vortexed (1 min), and sonicated (5 °C, 40 kHz, 30 min). After centrifugation (15,000× *g*, 4 °C, 15 min), the supernatant was dried under nitrogen and reconstituted in 100 μL of 50% acetonitrile. Repeat the vortex, sonication, and centrifugation steps described above, and the final supernatant was injected.

LC–MS/MS analysis: An ExionLC AD system coupled to a SCIEX QTRAP 6500+ mass spectrometer (ESI) was used. Separation employed a Waters BEH C18 column (150 × 2.1 mm, 1.7 μm) at 50 °C with 5 μL injection. Mobile phase: 0.1% formic acid in water (A) and acetonitrile (B), flow rate 0.4 mL/min. Gradient: 0–0.5 min, 5–10%B; 0.5–1.0 min, 10–20%B; 1.0–2.0 min, 20–28%B; 2.0–8.0 min, 28%B; 8.0–11.0 min, 28–33%B; 11.0–20.0 min, 33–45%B; 20.0–23.0 min, 45–50%B; 23.0–29.0 min, 50–80%B; 29.0–29.01 min, 80–100%B; 29.01–31.0 min, 100%B; 31.0–31.01 min, 100–5%B; 31.01–33.0 min, 5%B. ESI settings: TEM 550 °C, IS –4500 V, CUR 35 psi, GS1/GS2 50 psi. Data were processed with Analyst software for integration, calibration, and quantification.

2.11. RT-qPCR

Liver samples were used to extract RNA by employing the Trizol reagent and reverse-transcribed into cDNA with the HiScript III 1st Strand cDNA Synthesis Kit (Lot: R312-01, Nuovezan, China). Quantitative PCR was conducted on an ABI 7500 Manager V2.0.4 instrument (Thermo Fisher Scientific, Waltham, MA, USA), employing a standard thermal cycling protocol. GAPDH served as the normalization control, and gene expression quantification was based on the $2^{-\Delta\Delta Ct}$ method, with specific primers detailed in Table S1.

2.12. Western Blotting

The Western blotting analysis started by lysing liver tissue in RIPA buffer (Lot: WB0003, TDY, China), which included 1% PMSF and a protein phosphatase inhibitor. The homogenized sample was then centrifuged to collect the supernatant. Concentrations of proteins were determined utilizing a BCA kit, and samples were prepared by mixing them with buffer and subsequently subjected to denaturation through heating. After undergoing SDS-PAGE, the proteins were transferred to a PVDF membrane, which was then blocked and washed. A suite of antibodies, including FXR, CYP7A1, BSEP, MRP2, and GAPDH, were applied to the membrane overnight at 4 °C. Following the washing process, secondary antibodies were introduced, and the bands that formed were captured. Image J was used to analyze the intensities of the bands, with GAPDH being used as the standard for normalization.

2.13. Statistical Analysis

GraphPad™ Prism 8.0 (GraphPad Software, Boston, MA, USA), Origin 2021 (OriginLab, Northampton, MA, USA) and Microsoft Excel (version 2019, Microsoft, USA) were used to perform the statistical analysis and generate the visual representations. The orthogonal partial least-squares discriminant analysis (OPLS-DA) was executed utilizing SIMCA-P software (Version 14.1, Umetrics, Malmö, Sweden). Multigroup comparisons were made using one-way ANOVA followed by the least significant difference test, and the threshold for statistical significance was set at $p < 0.05$. Daily body-weight data were analyzed using two-way repeated-measures ANOVA (group ×

time), followed by Bonferroni-corrected post hoc comparisons, to account for the repeated observations obtained from the same animals. To test the central claim that vinegar processing enhances the effect of Qingpi, raw vs. processed Qingpi were compared directly at matched doses (LR-QP vs. LV-QP and HR-QP vs. HV-QP) by pre-planned pairwise contrasts within the one-way ANOVA model, and the corresponding effect sizes (mean differences or Cohen's *d*) with 95% confidence intervals are reported. Post hoc significance levels are indicated as * $p < 0.05$, ** $p < 0.01$ and *** $p < 0.001$ in the figures. All data are presented as mean ± SD.

3. Results

3.1. Effects of Raw and Vinegar-Processed Qingpi on Cholestatic Liver Injury in Rats

Following ANIT-induced CLD modeling, rats developed typical cholestatic symptoms, including ruffled and dull fur, reduced appetite, and dark urine [24]. As shown in Figure 1B, a significant decrease in body weight was observed in the model group compared with the control group from day 5 onward. This weight loss was attenuated in all Qingpi intervention groups. Notably, the UDCA, HR-QP, and HV-QP groups all exhibited significant weight recovery compared with the model group ($p < 0.05$ for HR-QP and $p < 0.01$ for UDCA and HV-QP). Consistent with these findings, the liver coefficient results (Figure 1C) revealed that the UDCA, HR-QP, and HV-QP groups each achieved a significant reduction relative to the model group (all $p < 0.05$) and the liver coefficient in the HV-QP group was significantly lower than that in the HR-QP group ($p < 0.05$), while the difference between the HV-QP and UDCA groups was not statistically significant.

Then we next examined whether Qingpi could restore bile excretion—a direct indicator of cholestasis resolution. As presented in Figure 1D, bile volume flow was significantly decreased in the model group versus the control group ($p < 0.05$), confirming the presence of biliary obstruction. Following intervention of raw and vinegar-processed Qingpi, this parameter was significantly elevated relative to the model group ($p < 0.05$), indicating effective relief of cholestatic obstruction. Among the Qingpi groups, bile volume flow was highest in the HV-QP group and was significantly higher than that in the HR-QP group ($p < 0.01$), supporting a processing-related improvement in this endpoint.

Histological examination with HE staining (Figure 1E) showed that liver tissues in the control group maintained intact hepatic cord structures with orderly arranged hepatocytes. In contrast, the model group exhibited severe hepatic injury, characterized by disrupted lobular architecture, hepatocellular steatosis, and inflammatory cell infiltration. In the Qingpi-pretreated groups, particularly the HV-QP group, these histopathological alterations appeared on descriptive assessment to be less pronounced than in the model group, with morphological features broadly similar to those observed in the UDCA group.

Beyond the improvements in systemic symptoms and hepatic morphology, serum levels of liver function-related biomarkers (ALT, AST, ALP, TBA, DBIL, and TBIL) were measured to further evaluate the effects of Qingpi on CLD rats [25]. As depicted in Figure 1F, the model group exhibited markedly elevated levels of all six biochemical parameters compared with the control group, further confirming successful CLD model establishment. Following intervention with Qingpi, all six biomarkers were reduced relative to the model group, and the reductions reached statistical significance at $p < 0.05$ in most treatment–marker comparisons and at $p < 0.01$ in several of them (Figure 1F). A dose-dependent trend was observed, as the high-dose groups (HR-QP and HV-QP) generally exhibited lower biomarker levels than the low-dose groups (LR-QP and LV-QP). Direct comparison of the raw and vinegar-processed forms at matched doses showed that the HV-QP group exhibited significantly lower levels of ALP and TBA than the HR-

QP group ($p < 0.05$ and $p < 0.01$, respectively), supporting a processing-related improvement in these markers.

Collectively, these results indicated that both raw and vinegar-processed Qingpi extracts alleviated cholestatic symptoms, attenuated body weight loss, reduced the liver coefficient, restored bile volume flow and decreased serum biochemical markers of hepatic injury in ANIT-induced CLD rats. Importantly, the vinegar-processed form exhibited a superior ameliorative effect compared to the raw form, highlighting the impact of traditional processing on its health-promoting properties.

3.2. Chemical Profiling and Differential Components of Raw and Vinegar-Processed Qingpi

UPLC-Q-TOF-MS analysis was performed on raw and vinegar-processed Qingpi extracts (Figure 2A). Total ion chromatograms were acquired in both positive and negative ion modes (Figure S1). Through systematic matching of molecular formulae, accurate masses, retention times, fragment ions, and reference standards, a total of 52 chemical components were characterized, comprising 36 flavonoids (15 flavonols, 7 flavanones and 14 flavones), 3 alkaloids, 6 organic acids, 1 coumarin, 1 terpene and 5 other constituents. Of these, 9 compounds were confirmed with authentic reference standards by comparing their retention times and MS/MS fragmentation patterns with those of the standards. The remaining compounds were putatively annotated based on accurate mass measurements, diagnostic MS/MS fragments, and matching with online databases (detailed in Table S2).

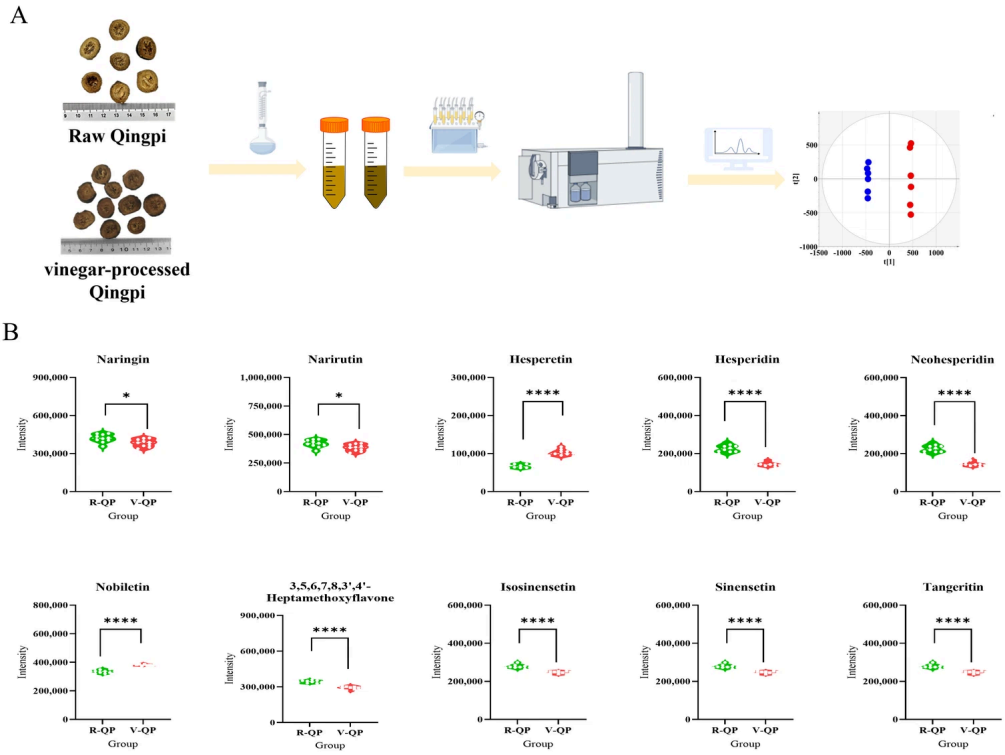
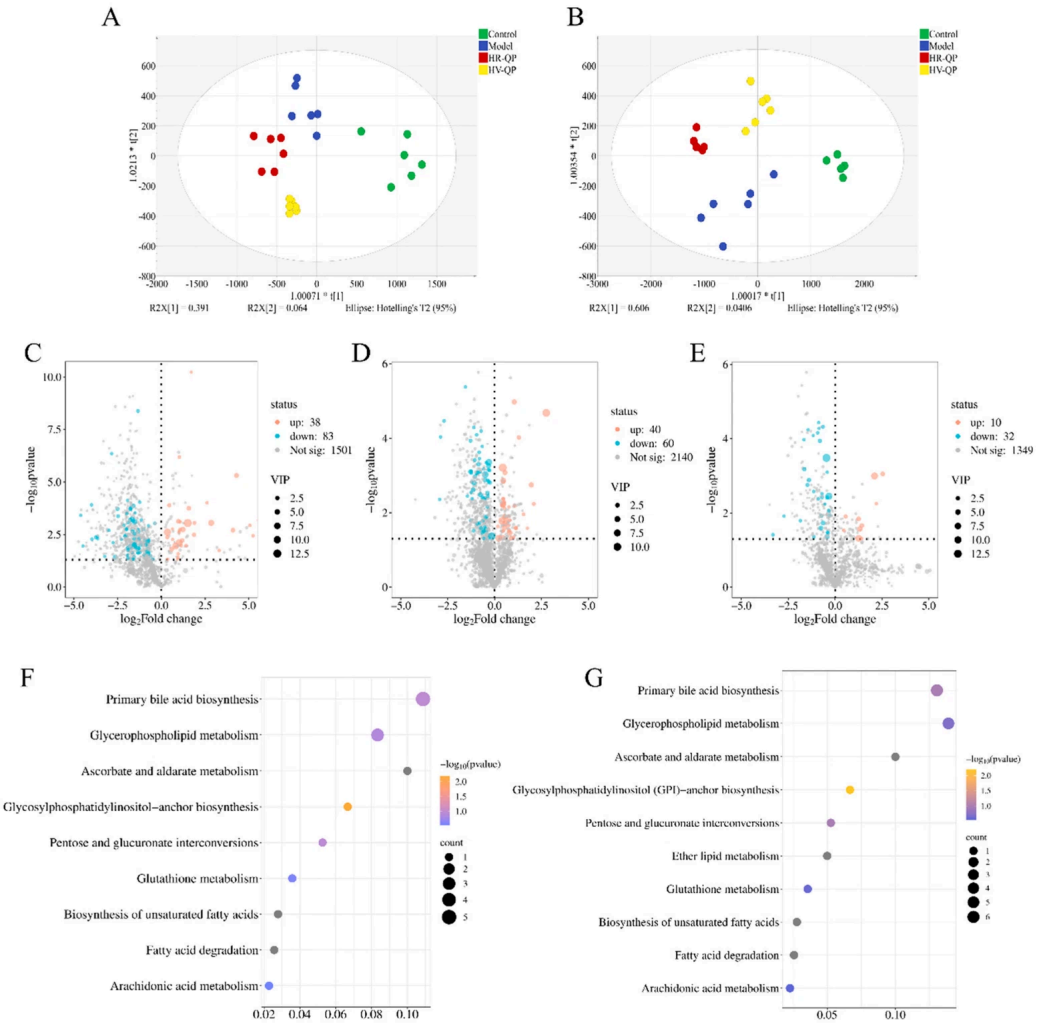


Figure 2. Chemical profiling and differential components of raw and vinegar-processed Qingpi. (**A**) Schematic diagram of the UPLC-Q-TOF-MS analysis workflow. (**B**) Relative intensities of the 10 potential quality differential components. Extracts were prepared from three independent processing replicates per group ($n = 3$). Data are presented as mean ± SD. * $p < 0.05$, **** $p < 0.0001$ between two groups.

Multivariate statistical analyses were employed to evaluate the chemical differentiation induced by vinegar processing. PCA revealed clear clustering and distinct separation between raw and vinegar-processed Qingpi groups (Figure S2A), indicating substantial chemical differentiation induced by the vinegar-processing procedure. The subsequent OPLS-DA model, which exhibited excellent stability and predictive capability (R^2X = 0.854, R^2Y = 0.992, Q^2 = 0.973; permutation test in Figure S2B), further validated this effective differentiation (Figure S2C,D). Based on chemometric screening and *t*-test analysis, 10 differential components were screened. Among these, hesperetin and nobiletin were significantly elevated in V-QP, whereas eight components, including naringin, were markedly decreased (Figure 2B). These values are based on three independent processing replicates per group (n = 3) with peak areas normalized to sample weight, and thus represent relative signal intensities rather than absolute contents. Notably, as most of these differential components belong to the flavonoid class, the compositional changes induced by vinegar processing are primarily reflected in the flavonoid profile of Qingpi.

3.3. Serum Metabolomic Analysis of Qingpi Intervention in Cld Rats

Following peak alignment and normalization, the processed data were imported into SIMCA 14.1 for pattern recognition. Clear group separations were observed in the PLS-DA (Figure 3A,B) and OPLS-DA score plots (Figure S3). Volcano plot analysis revealed significant metabolic disturbances in the model group relative to the control group (121 differential metabolites; Figure 3C). Intervention with Qingpi effectively reversed these disturbances, with 100 and 42 metabolites showing significant alterations in the HR-QP (Figure 3D) and HV-QP (Figure 3E) groups, respectively. By cross-referencing with online databases, 24 endogenous metabolites were putatively annotated as potential CLD-related biomarkers associated with Qingpi intervention (Table S3).



https://doi.org/10.3390/foods15234312

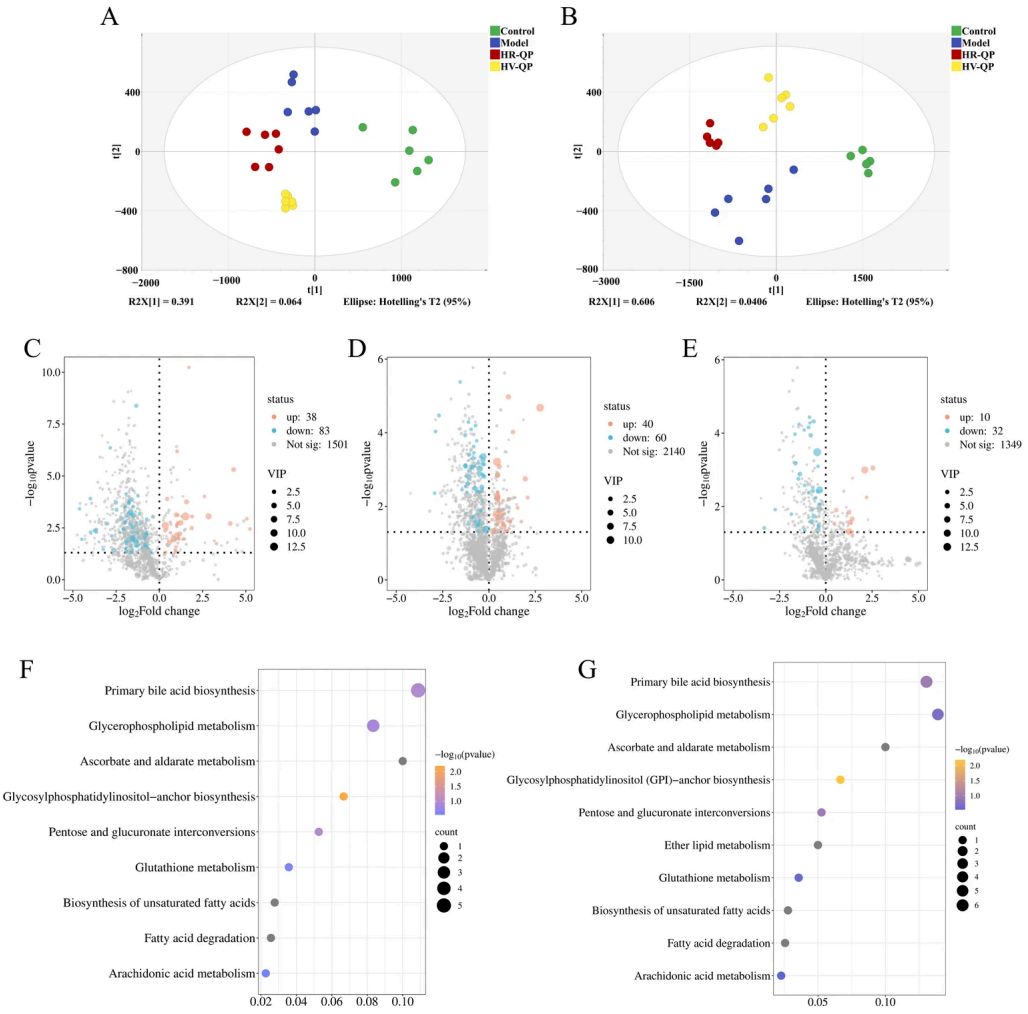


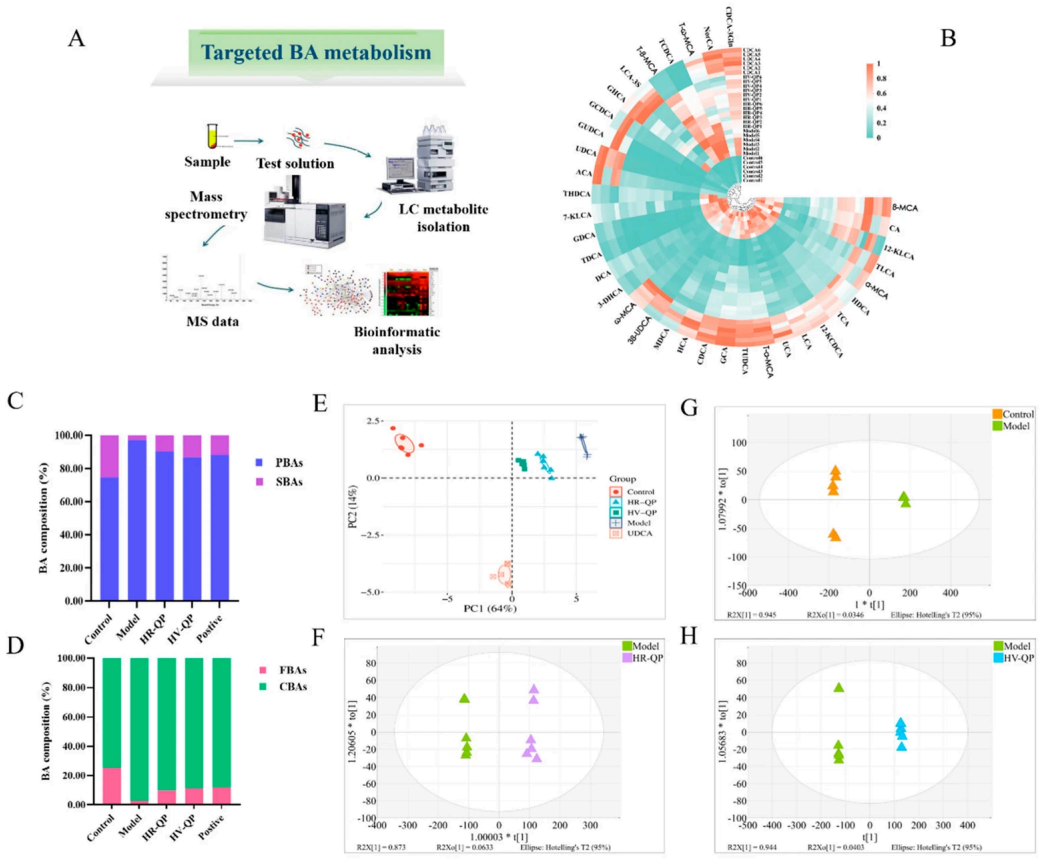
Figure 3. Effect of Qingpi on the serum metabolomic profiling of CLD rats. (**A**,**B**) PLS-DA score scatter plots in negative and positive ion modes. (**C**–**E**) Volcano plots of the metabolic profiles from the different groups (Control vs. Model, HR-QP vs. Model, and HV-QP vs. Model). (**F**,**G**) Bubble maps of the KEGG metabolic pathway enrichment.

KEGG pathway enrichment analysis further revealed that both raw and vinegar-processed Qingpi significantly modulated several metabolic pathways, most notably primary bile acid biosynthesis, as well as glycerophospholipid metabolism, pentose and glucuronate interconversions, glutathione metabolism, and arachidonic acid metabolism (Figure 3F,G). Collectively, these results indicate that both raw and vinegar-processed Qingpi interventions effectively alleviate metabolic disturbances in CLD rats, with their ameliorative effects closely associated with the regulation of these pathways, particularly primary bile acid biosynthesis.

3.4. Modulation of Bile Acid Profiles by Raw and Vinegar-Processed Qingpi

Targeted metabolomics was employed to analyze serum bile acid levels and assess the regulatory effects of Qingpi (Figure 4A). A targeted LC-MS approach covering 47 bile acids was applied to analyze serum samples from the control, model, UDCA, HR-QP, and HV-QP groups (ion-pairing parameters are detailed in Table S4). A mixed standard solution of 50 ng·mL^{-1} was prepared as a quality control (QC) sample for methodological validation. The results demonstrated that the analytical system exhibited good linearity, stability, precision, and accuracy (Tables S5–S7), making it suitable for quantitative detection. Finally, a total of 35 bile acids were quantitatively detected in the serum sam-

ples (Table S8). The heatmap (Figure 4B) provided a comprehensive view of the altered bile acid profiles, revealing distinct clustering trends across the different groups. In the control group, most primary and secondary bile acids (e.g., CA, β-MCA, DCA, and LCA) showed relatively high abundances. However, ANIT-induced cholestasis triggered a severe disruption in the model group, characterized by a widespread depletion of these major circulating bile acids and a massive accumulation of TCDCA and T-β-MCA. This redistribution of the serum bile acid pool is consistent with impaired bile acid homeostasis. Strikingly, interventions with raw Qingpi, vinegar-processed Qingpi, and UDCA all markedly reversed these pathological shifts, with their abundance patterns exhibiting a clear trajectory back toward the control group.



https://doi.org/10.3390/foods15234312

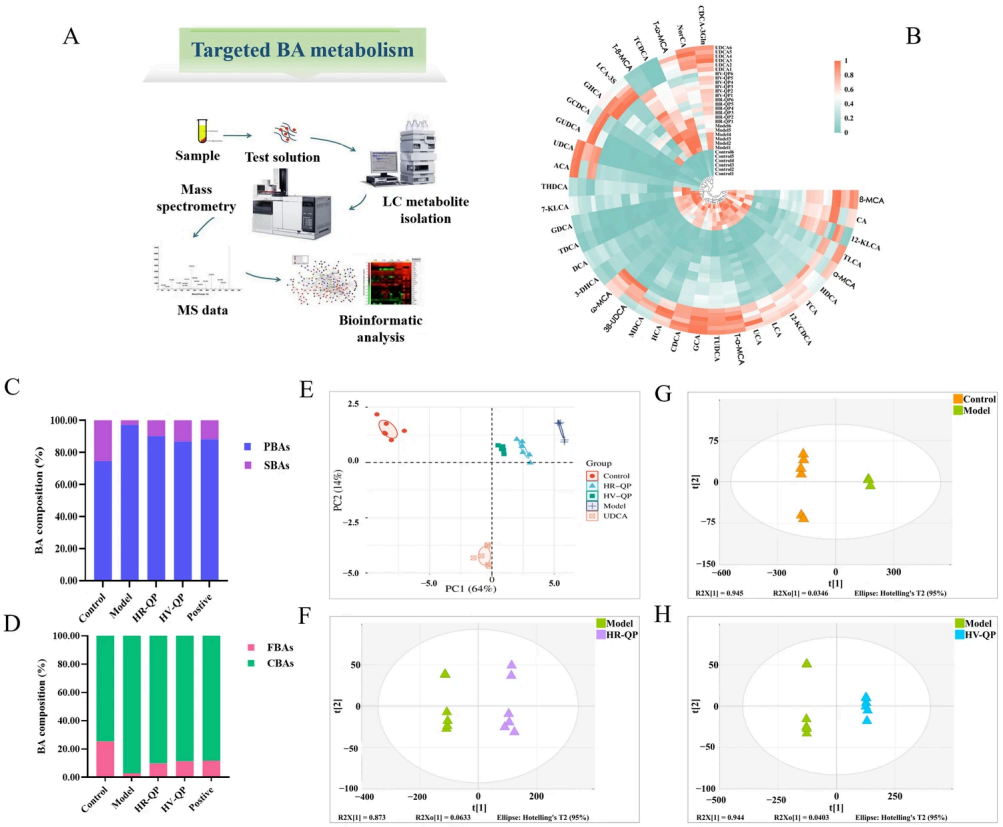


Figure 4. Targeted bile acid metabolomics analysis in CLD rats following Qingpi intervention. (**A**) Schematic workflow of the targeted bile acid metabolomics analysis. (**B**) Heatmap of bile acids across different groups. (**C**) Compositional proportions of PBAs vs. SBAs. (**D**) Compositional proportions of CBAs vs. FBAs) (**E**) PCA score plot. (**F**–**H**) Pairwise OPLS-DA score plots.

To further evaluate the impact of cholestasis on bile acid biotransformation, we analyzed the compositional ratios of primary bile acids (PBAs) versus secondary bile acids (SBAs), as well as conjugated (CBAs) versus free bile acids (FBAs) (Figure 4C,D). These ratios reflect the composition of the circulating bile acid pool and can provide indirect evidence for changes in hepatic synthesis, intestinal microbial conversion, hepatic detoxification or biliary efflux. Consistent with the heatmap (Figure 4B), the model group exhibited significantly elevated proportions of PBAs and CBAs, which was driven by the abnormal accumulation of PBAs (specifically TCDCA and T-β-MCA) alongside the severe depletion of eight PBAs (CA, GCA, TCA, CDCA, β-MCA, T-α-MCA, TUDCA, α-MCA) and six SBAs (DCA, THDCA, HDCA, LCA, TLCA, 12-KLCA). These changes in serum ratios suggest a severe impairment in the intestinal conversion of primary to secondary bile acids and alterations in hepatic conjugation/excretion processes. However, intervention with both raw and vinegar-processed Qingpi effectively restored these ratios toward control levels, demonstrating their regulatory capacity on the serum bile acid pool and overall bile acid homeostasis. Furthermore, PCA (Figure 4E) was applied to visualize the global variations in the 35 quantified bile acids across all groups, showing distinct clustering and clear separation among the control, model, and intervention groups. To further pinpoint the specific differences, pairwise OPLS-DA models (Figure 4 F–H) were constructed between the control and model groups, as well as between the model group and each intervention group (HR-QP and HV-QP). These models clearly separated the bile acid profiles of the respective two groups, demonstrating significant alterations in the serum bile acid profile following ANIT induction and the subsequent

Qingpi interventions.

To evaluate the differential regulatory effects of raw and vinegar-processed Qingpi on specific bile acids, a combined set of differential bile acids (a union of 15 targets identified from HR-QP vs. Model and HV-QP vs. Model comparisons) was visualized using box plots (Figure 5). The quantitative data for these 15 bile acids correspond directly to the values in Table S8. In these plots, the horizontal line within each box represents the median; the top and bottom edges of the box indicate the 75th and 25th percentiles (interquartile range, IQR), respectively; and the whiskers extend to the minimum and maximum values. Both forms of Qingpi effectively restored the markedly depleted primary and secondary bile acids (e.g., CA, TCA, and DCA) and significantly decreased the abnormally elevated TCDCA and T-β-MCA. Notably, vinegar processing significantly enhanced this regulatory capacity. A direct comparison between the two Qingpi forms revealed that the vinegar-processed group (HV-QP) exhibited significantly stronger effects on six key bile acids. Specifically, HV-QP showed a more pronounced restoration of CA, TCA, TUDCA, and 12-KLCA, and a stronger reduction in TCDCA and T-β-MCA compared to the raw form (HR-QP). These results indicate that vinegar processing enhances the ability of Qingpi to modulate the serum bile acid pool and to attenuate the accumulation of bile acids elevated under ANIT-induced cholestasis.

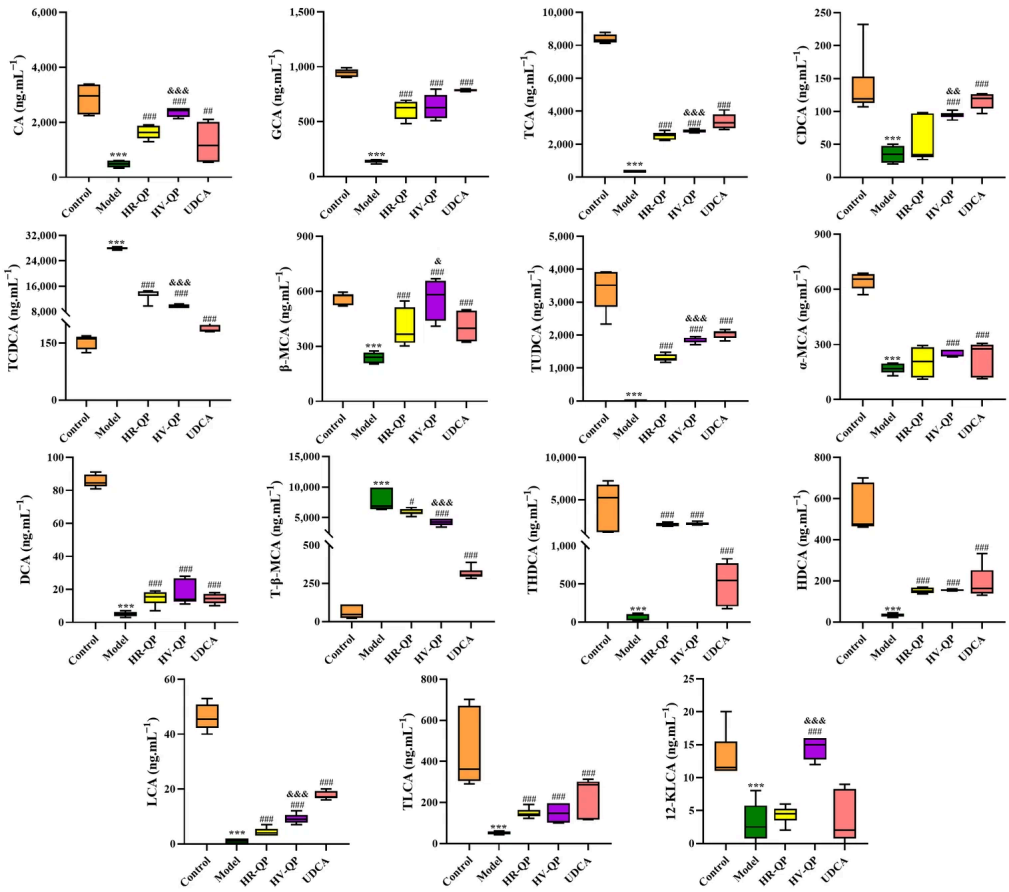


Figure 5. Box plots of the combined differential bile acids identified from the HR-QP vs. Model and HV-QP vs. Model comparisons, illustrating the responses to raw and vinegar-processed Qingpi interventions. Data are expressed as mean ± SD (n = 6). *** $p < 0.001$ vs. control group; # $p < 0.05$, ## $p < 0.01$, ### $p < 0.001$ vs. model group; & $p < 0.05$, && $p < 0.01$, &&& $p < 0.001$ vs. HR-QP group.

3.5. Modulation of the Fxr Signaling Pathway by Qingpi in Cld Rats

Considering that FXR acts as the primary bile acid sensor and a master regulator of homeostasis, we next examined the effects of Qingpi on this signaling pathway. FXR governs the transcriptional control of key downstream genes involved in bile acid synthesis (CYP7A1) and efflux transport (BSEP and MRP2). Accordingly, the mRNA and protein expression levels of FXR, CYP7A1, BSEP, and MRP2 were examined in the liver tissues using RT-qPCR and Western blotting. As shown in Figure 6, ANIT induction significantly suppressed the mRNA expression of FXR, BSEP, and MRP2, while markedly elevating CYP7A1 levels ($p < 0.001$). Intervention with both forms of Qingpi effectively reversed these trends, significantly upregulating FXR, BSEP, and MRP2, and downregulating CYP7A1. Western blotting further confirmed these regulatory effects at the protein level ($p < 0.05$, $p < 0.01$ $p < 0.001$, Figure 7). At the protein level, both HR-QP and HV-QP increased FXR ($p < 0.01$), BSEP ($p < 0.001$) and MRP2 ($p < 0.05$) expression and decreased CYP7A1 expression ($p < 0.001$) relative to the model group, and HV-QP further increased FXR and BSEP expression relative to HR-QP ($p < 0.05$ for both). The HV-QP versus HR-QP differences for CYP7A1 and MRP2 were not statistically significant. At the mRNA level, the HV-QP group showed significantly higher FXR expression and a stronger reduction in CYP7A1 than the HR-QP group ($p < 0.001$ for both), identifying these transcriptional changes as endpoints supporting processing-related superiority. These expression changes indicate an association between Qingpi intervention and the FXR pathway.

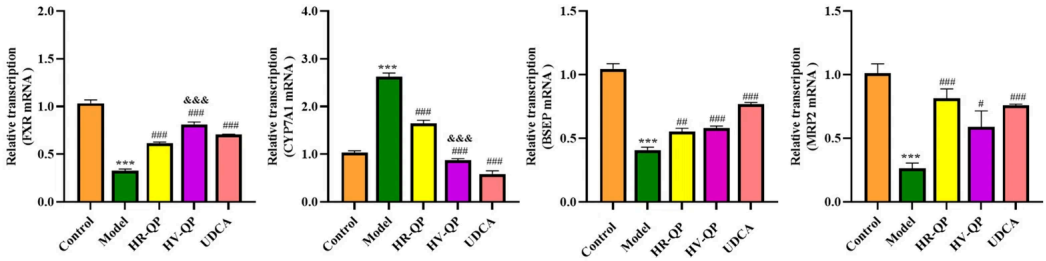


Figure 6. Effect of Qingpi intervention on the mRNA expression levels of FXR signaling pathway-related genes in CLD rats. Data are expressed as mean ± SD ($n = 3$). *** $p < 0.001$ vs. control group; # $p < 0.05$, ## $p < 0.01$, ### $p < 0.001$ vs. model group; &&& $p < 0.001$ vs. HR-QP group.

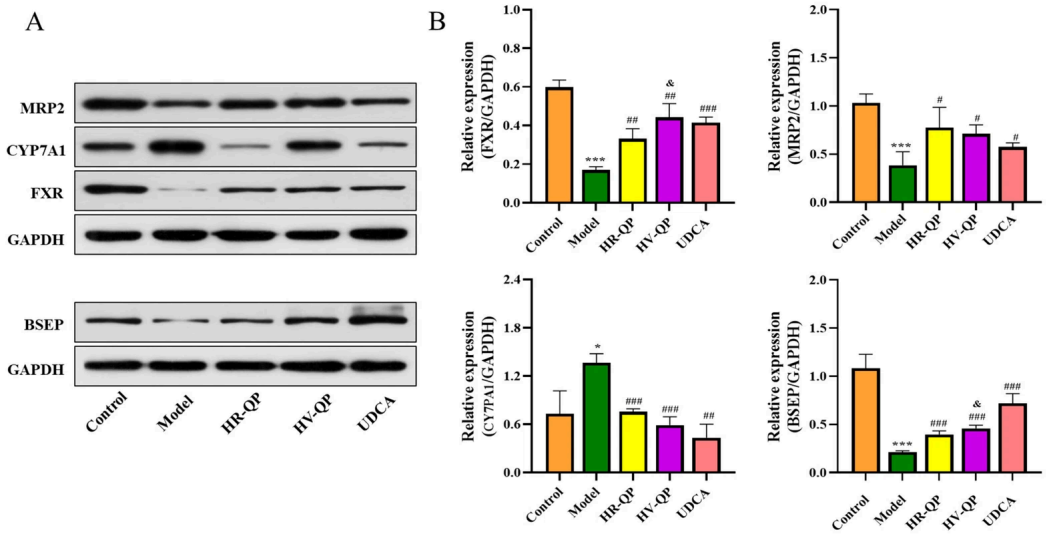


Figure 7. Effect of Qingpi intervention on the protein expression levels of FXR signaling pathway-related genes in CLD rats. (**A**) Western blot bands showing the protein expression of MRP2,

CYP7A1, FXR, and BSEP in the liver of rats in each group (GAPDH was used as the internal control); (**B**) Quantitative analysis (bar graphs) of the relative expression levels of FXR signaling pathway-related proteins (FXR, MRP2, CYP7A1, BSEP). Data are expressed as mean ± SD (n = 3). * p < 0.05, *** p < 0.001 vs. Control group; # p < 0.05, ## p < 0.01, ### p < 0.001 vs. Model group; & p < 0.05 vs. HR-QP group.

By integrating the targeted bile acid metabolomics with the FXR pathway analysis, the links between bile acid metabolism and FXR signaling were revealed. ANIT stimulation disrupted the bile acid profile and reduced FXR expression, which was accompanied by elevated CYP7A1 expression and reduced BSEP/MRP2 levels, consistent with impaired bile acid transport and intrahepatic accumulation. Intervention with both raw and vinegar-processed Qingpi restored FXR expression, downregulated CYP7A1-mediated synthesis, and upregulated BSEP/MRP2-mediated efflux. These measured expression changes are consistent with the restoration of FXR-mediated regulation and with improved bile acid homeostasis. Mechanistically, the restoration of total FXR expression by Qingpi may provide the protein basis for its transcriptional function, and the concurrent reversal of downstream target genes, namely the downregulation of CYP7A1 and the upregulation of BSEP/MRP2, is consistent with the restoration of the FXR-mediated transcriptional signaling pathway. Notably, the higher FXR expression induced by vinegar-processed Qingpi corresponded to its greater effect on the serum bile acid profile, suggesting a greater potential for FXR-related downstream responses, and this provides a working explanation for the enhanced alleviation of cholestasis by vinegar processing.

4. Discussion

Cholestatic liver disease encompasses a spectrum of disorders driven by intrahepatic bile acid accumulation and impaired bile flow, representing a substantial clinical challenge with limited effective therapies [1,26]. These limitations have motivated growing interest in dietary and food-derived interventions that may modulate bile acid metabolism and reduce the risk of cholestatic progression. Qingpi, a traditional culinary and medicinal material, has attracted attention for its health-promoting properties [11,27,28]. In the present study, we characterized 52 components from Qingpi extracts, with flavonoids constituting the predominant chemical class [29]. Multivariate analyses revealed robust separation between raw and vinegar-processed samples, confirming that vinegar processing, a common food-processing technique, significantly alters Qingpi's flavonoid composition. The increased levels of hesperetin and nobiletin, alongside the reduction in glycosides like naringin, suggest that processing may enhance the functional potential of this food ingredient. Notably, Qingpi holds a dual identity in traditional Chinese practice. The present study focuses on its chemical basis and the influence of processing as they relate to its food use, providing a chemical and mechanistic basis for its application as a functional food ingredient.

Animal models are essential for evaluating the health-related effects of dietary ingredients [24]. ANIT-induced liver injury closely mimics human intrahepatic cholestasis by primarily targeting biliary epithelial cells, leading to bile duct obstruction and subsequent hepatocellular damage [30]. In our study, the model group exhibited significantly reduced bile volume flow and markedly elevated serum liver function markers, confirming successful CLD model establishment [25]. Intervention with both raw and vinegar-processed Qingpi reversed these abnormalities, effectively alleviating liver injury and metabolic disturbances. Crucially, the vinegar-processed form exhibited superior efficacy, suggesting that traditional processing enhances the hepatoprotective potential of Qingpi as a dietary ingredient.

Bile acids are synthesized in the liver from cholesterol and act as signaling mole-

cules to regulate their own synthesis and transport, maintaining homeostasis [31–34]. Under physiological conditions, the composition and proportion of bile acids remain stable. However, during cholestasis, this homeostasis is disrupted. Elevated bile acids become cytotoxic and have been linked to inflammation, fibrosis, and ultimately liver failure [35–37]. In our study, targeted metabolomics revealed that ANIT stimulation significantly altered the bile acid profile. Both raw and vinegar-processed Qingpi effectively modulated bile acid composition and restored the balance between PBAs/SBAs and CBAs/FBAs, reflecting a redistribution of the circulating bile acid pool. The contribution of individual bile acids to this process is not uniform, and their biological effects depend on the biological or pathological context. The change in T-β-MCA levels may be related to its biological activity as an FXR antagonist. These changes in ratios indicate altered bile acid homeostasis, but do not directly quantify any single metabolic process. Serum levels represent an integrated outcome of hepatic synthesis, hepatic transport, and intestinal microbial conversion. Deconjugation is mediated mainly by intestinal microbial bile salt hydrolases, whereas hepatic handling mainly involves conjugation and biliary excretion. Therefore, the serum bile acid ratios observed here reflect the overall distribution of the circulating pool rather than specific rates of hepatic or microbial metabolism. The vinegar-processed form showed a stronger regulatory capacity on specific bile acids that were elevated under cholestatic conditions (e.g., TCDCA and T-β-MCA), highlighting the impact of processing on its bile acid-modulating properties at the level of the serum bile acid pool.

The combination of untargeted and targeted metabolomics emphasizes the importance of bile acid metabolic pathways. It is widely reported that Farnesoid X Receptor (FXR) is centrally located in the homeostatic regulation of bile acids [38–41]. In the canonical pathway, FXR activation induces small heterodimer partner (SHP) expression, which subsequently downregulates CYP7A1 and reduces bile acid synthesis [42]. Cholestasis is also associated with dysregulation of transporters such as BSEP and MRP2 [43,44]. BSEP primarily transports bile salts through hepatocyte bile duct membranes, and inhibition leads to progressive intrahepatic cholestasis, and FXR binds directly to a response element on the BSEP promoter [45]. MRP2 is an important transport carrier protein on the plasma membrane of the bile duct surface and mediates the efflux of bile acids [46]. FXR can accelerate bile acid transport and excretion by regulating MRP2, BSEP expression [14,47]. In the present study, we revealed that raw and vinegar-processed Qingpi restored FXR expression levels, downregulated CYP7A1, and upregulated BSEP and MRP2 (Figure 8). These transcriptional changes support a potential association between the altered flavonoid profile of Qingpi and the FXR signaling pathway, although a direct molecular link between specific flavonoids and FXR modulation remains to be established. The higher FXR and BSEP expression observed with vinegar-processed Qingpi corresponded to its greater effect on the serum bile acid profile, indicating a stronger response at the level of FXR-related markers. Whether this reflects enhanced FXR activation remains to be further verified. In summary, the current findings support a hypothesis that Qingpi is associated with FXR-related changes in CYP7A1, BSEP and MRP2 expression and with improved serum bile acid homeostasis, and vinegar processing is associated with a greater effect on these endpoints.

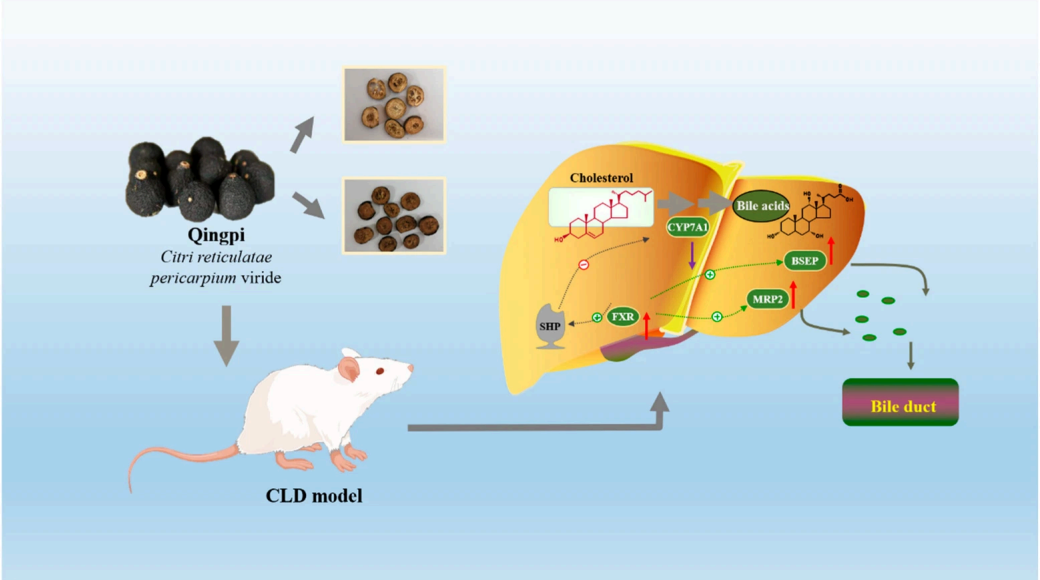


Figure 8. Schematic illustration of the FXR signaling pathway associated with Qingpi intervention. Red and green arrows indicate the measured up- and downregulation of mRNA/protein expression, respectively. SHP (gray) is a literature-known intermediate not measured in this study.

While the results suggest that Qingpi can offer a dietary avenue for alleviating ANIT-induced CLD through FXR signaling, several limitations should be acknowledged. Firstly, owing to the complex pathogenesis of cholestasis, a single ANIT model may only simulate specific pathological mechanisms. ANIT can primarily induce acute cholangiocyte injury and biliary obstruction, which mostly resembles human intrahepatic cholestasis (such as drug-induced liver injury or primary biliary cholangitis), but it fails to fully replicate the chronic progressive features of other forms of cholestasis, such as primary sclerosing cholangitis or genetic transporter defects. Therefore, exploring multiple models (e.g., BDL or genetic models) could further validate these findings. Secondly, the experimental extracts differ significantly from conventional food preparations (e.g., dietary decoctions or powders) in terms of concentration and administration route. The actual intake of bioactive flavonoids from conventional food sources may be limited by their oral bioavailability. Further studies are required to investigate the pharmacokinetics and absorption of these compounds under realistic dietary consumption scenarios. Comprehensive long-term safety evaluations and toxicological studies are essential to substantiate the safe use of vinegar-processed Qingpi as a food ingredient. Thirdly, there are species-specific differences in bile acid metabolism between rats and humans. Rats primarily synthesize muricholic acids (α-, β-, and ω-MCA) and have a high proportion of taurine-conjugated bile acids, whereas humans predominantly produce chenodeoxycholic acid and cholic acid, with glycine conjugation being more prevalent. These compositional differences indicate that the findings should be cautiously extrapolated to humans, and future studies could employ humanized models or human hepatocyte cultures to confirm these FXR-mediated regulatory effects. In addition, future research should investigate the effects of Qingpi's volatile oil and other active constituents, as well as the exact direct molecular targets and the interplay of multiple pathways. Furthermore, subsequent studies should analyze bile acid compositions in bile, urine, and feces to provide a more comprehensive view. In summary, the current findings provide preclinical evidence for the potential of vinegar-processed Qingpi in modulating bile acid metabolism, and clarify how traditional vinegar processing enhances this biological activity, though further research is needed to address these limitations.

5. Conclusions

In summary, this study demonstrates that both raw and vinegar-processed Qingpi effectively alleviate ANIT-induced cholestatic liver injury, as evidenced by improved bile flow, restored liver function, and attenuated histopathological damage. Vinegar processing significantly enhanced these ameliorative effects, which is closely associated with the processing-induced alterations in the flavonoid profile of Qingpi. Mechanistically, Qingpi intervention regulates FXR-mediated bile acid synthesis and efflux, maintaining bile acid homeostasis. These findings provide a robust chemical and mechanistic basis for the application of Qingpi as a functional food ingredient, and highlight traditional vinegar processing as an effective strategy to enhance its health-promoting potential.

Supplementary Materials: The following supporting information can be downloaded at: https://www.mdpi.com/article/doi/s1, Figure S1：Positive-negative ion plots of the high-resolution mass spectra of the extract of raw Qingpi (R-QP) and vinegar-processed Qingpi (V-QP)；Figure S2：Chemometrics analysis of the chromatographic data from raw and vinegar-processed Qingpi. (A) Score plot of PCA; (B) OPLS-DA permutation test results; (C) Score plot of OPLS-DA; (D) VIP scores. The modeling parameters (R^2X, R^2Y, and Q^2) are annotated at the top of each plot. The ellipses represent the 95% confidence intervals (Hotelling's T2)；Figure S3：The models represent pairwise comparisons: (A, B) Control vs. Model; (C, D) Model vs. HR-QP; (E, F) Model vs. HV-QP. The modeling parameters (R^2X, R^2Y, and Q^2) are annotated at the top of each plot. The ellipses represent the 95% confidence intervals (Hotelling's T2). Table S1：Primer sequence；Table S2：The 52 components characterized from Qingpi based on UPLC-Q-TOF-MS/MS；Table S3：Putative annotation of 24 metabolites in serum；Table S4：Bile acid pair parameter information；Table S5：Standard curve of mixed standard solution；Table S6：Stability results of bile acids in the QC samples；Table S7：Precision and accuracy in the QC samples；Table S8：Effect of raw and vinegar-processed Qingpi on bile acids content in rats ($ng.mL^{-1}$, $n = 6$, $x \pm s$).

Author Contributions: Q.Z.: writing—original draft, software, methodology, funding acquisition, conceptualization. M.L.: resources, data curation. R.X.: methodology, software, visualization. X.M.: data curation, formal analysis. L.S.: supervision, writing—review and editing. J.X.: resources, investigation. C.M.: supervision, writing—review and editing. G.Y.: project administration, writing—review and editing. T.L.: project administration, funding acquisition, writing—review and editing. All authors have read and agreed to the published version of the manuscript.

Funding: This study was supported by the National Natural Science Foundation of China (82505026, 82474078), the National Key R&D Program of China (NO. 2023YFC3504200), and the China Postdoctoral Science Foundation under Grant Number 2025M773925. Authors would like to thank all referees and the authors of all bibliographical references.

Institutional Review Board Statement: The study was conducted in accordance with the Declaration of Helsinki, and approved by the Ethics Committee of Nanjing University of Chinese Medicine (protocol code 202105A052 and date of approval 22 May, 2021).

Informed Consent Statement: Not applicable.

Data Availability Statement: The original contributions presented in this study are included in the article/supplementary material. Further inquiries can be directed to the corresponding authors.

Conflicts of Interest: The authors declare that the research was conducted in the absence of any commercial or financial relationships that could be construed as a potential conflict of interest.

Abbreviations

The following abbreviations are used in this manuscript.

ALP, alkaline phosphatase; ALT, alanine aminotransferase; AST, aspartate aminotransferase; ANIT, alpha-naphthyl isothiocyanate; BA, bile acid; BSEP, bile salt export pump; CA, cholic acid; CBAs, conjugated bile acids; CDCA, chenodeoxycholic acid; CLD, cholestatic liver disease; CYP7A1, cholesterol 7a-hydroxylase; DBIL, direct bilirubin; DCA, deoxycholic acid; ESI, electrospray ionization; FBAs, free bile acids; FXR, farnesoid X receptor; GAPDH, glyceraldehyde-3-phosphate dehydrogenase; GCA, glycocholic acid; HR-QP, high-dose administration of raw Qingpi; HV-QP, high-dose administration of vinegar-processed Qingpi; LR-QP, low-dose administration of raw Qingpi; LV-QP, low-dose administration of vinegar-processed Qingpi; MRP2, multidrug resistance-associated protein 2; OPLS-DA, orthogonal partial least-squares discriminant analysis; PBAs, primary bile acids; PCA, principal component analysis; QC, quality control; R-QP, raw Qingpi; SBAs, secondary bile acids; TBA, Total bile acid; TBIL, total bilirubin; TCM, Traditional Chinese Medicine; TCA, taurocholic acid; UDCA, ursodeoxycholic acid. V-QP, vinegar-processed Qingpi.

References

1. Woolbright, B.L.; Jaeschke, H. Inflammation and Cell Death During Cholestasis: The Evolving Role of Bile Acids. *Gene Expr.-J. Liver Res.* **2019**, *19*, 215–228. [Google Scholar] [CrossRef] [PubMed]
2. Bessone, F.; Hillotte, G.L.; Ahumada, N.; Jaureguizahar, F.; Medeot, A.C.; Roma, M.G. UDCA for Drug-Induced Liver Disease: Clinical and Pathophysiological Basis. *Semin. Liver Dis.* **2024**, *44*, 1–22. [Google Scholar] [CrossRef] [PubMed]
3. Gatzen, M.; Pausch, J. Treatment of cholestatic liver disease. *Med. Klin.* **2002**, *97*, 152–159. [Google Scholar]
4. Wei, C.L.; Qiu, J.; Wu, Y.Y.; Chen, Z.Q.; Yu, Z.W.; Huang, Z.C.; Yang, K.; Hu, H.L.; Liu, F. Promising traditional Chinese medicine for the treatment of cholestatic liver disease process (cholestasis, hepatitis, liver fibrosis, liver cirrhosis). *J. Ethnopharmacol.* **2022**, *297*, 115550. [Google Scholar] [CrossRef] [PubMed]
5. Jiang, Y.X.; Li, H.T.; Song, D.; Ye, P.H.; Xu, N.; Chen, Y.; Zhang, W.W.; Hu, Q.C.; Ma, X.; Wen, J.X.; et al. Comparative Evidence for Intrahepatic Cholestasis of Pregnancy Treatment With Traditional Chinese Medicine Therapy: A Network Meta-Analysis. *Front. Pharmacol.* **2021**, *12*, 774884. [Google Scholar] [CrossRef] [PubMed]
6. Commission, C.P. *Pharmacopoeia of the People's Republic of China*; China Medical Science Press: Beijing, China, 2020. [Google Scholar]
7. Gao, S.H.; Chen, X.J.; Yu, Z.Q.; Du, R.; Chen, B.Z.; Wang, Y.X.; Cai, X.T.; Xu, J.P.; Chen, J.M.; Duan, H.Y.; et al. Progress of research on the role of active ingredients of Citri Reticulatae Pericarpium in liver injury. *Phytomedicine* **2023**, *115*, 154836. [Google Scholar] [CrossRef] [PubMed]
8. Luo, M.; Luo, H.; Hu, P.; Yang, Y.; Wu, B.; Zheng, G. Evaluation of chemical components in Citri Reticulatae Pericarpium of different cultivars collected from different regions by GC-MS and HPLC. *Food Sci. Nutr.* **2018**, *6*, 400–416. [Google Scholar] [CrossRef]
9. Zhang, Q.; Xue, R.; Mei, X.; Su, L.; Zhang, W.; Li, Y.; Xu, J.; Mao, J.; Mao, C.; Lu, T. A study of volatiles of young citrus fruits from four areas based on GC-MS and flash GC e-nose combined with multivariate algorithms. *Food Res. Int.* **2024**, *177*, 113874. [Google Scholar] [CrossRef] [PubMed]
10. Barreca, D.; Gattuso, G.; Bellocco, E.; Calderaro, A.; Trombetta, D.; Smeriglio, A.; Laganà, G.; Daglia, M.; Meneghini, S.; Nabavi, S.M. Flavanones: Citrus phytochemical with health-promoting properties. *Biofactors* **2017**, *43*, 495–506. [Google Scholar] [CrossRef] [PubMed]
11. Zhang, Q.; Xu, R.J.; Xue, R.; Mei, X.; Qin, Y.W.; Shen, K.; Xu, J.G.; Su, L.L.; Mao, C.Q.; Xie, H.; et al. Ultra-high-performance liquid chromatography-quadrupole-time of flight-mass spectrometry combined with network pharmacology for analysis of potential quality markers of three processed products of Qingpi. *J. Sep. Sci.* **2024**, *47*, 2300281. [Google Scholar]
12. Chen, W.S.; Huang, P.L.; Chen, B. Analysis of the Effect of Processing on the Volatile Oil Composition of Qingpi by GC-MS. *China J. Chin. Mater. Medica* **2005**, *30*, 1388–1389. [Google Scholar]
13. Min, X.Q.; Meng, X.H. Overview of Processing Research on Qingpi slice. *China J. Chin. Mater. Medica* **2005**, *30*, 956–958. [Google Scholar]
14. Zhang, G.; Sun, X.; Wen, Y.; Shi, A.; Zhang, J.; Wei, Y.; Wu, X. Hesperidin alleviates cholestasis via activation of the farnesoid X receptor in vitro and in vivo. *Eur. J. Pharmacol.* **2020**, *885*, 173498. [Google Scholar] [CrossRef] [PubMed]
15. Chiang, J.Y.L. Bile Acid Metabolism and Signaling. *Compr. Physiol.* **2013**, *3*, 1191–1212. [Google Scholar] [CrossRef]

16. Bass, L.M.; Mollodi, P.; Whitington, P.F. Fxr Response in Cholestatic Liver Disease. *Hepatology* **2008**, *48*, 668a. [Google Scholar]
17. Han, B.; Kim, B.K.; Kim, K.; Fang, S. Essential roles of bile acids and their nuclear receptors, FXR and PXR, in the cholestatic liver disease. *Anim. Cells Syst.* **2016**, *20*, 175–178. [Google Scholar] [CrossRef]
18. Zhang, Z.Y.; Guan, G.Q.; Tang, Z.X.; Wan, W.M.; Huang, Z.P.; Wang, Y.F.; Wu, J.Z.; Li, B.; Zhong, M.L.; Zhang, K.F.; et al. Desmodium styracifolium (Osb.) Merr. Extracts alleviate cholestatic liver disease by FXR pathway. *J. Ethnopharmacol.* **2025**, *337*, 118972. [Google Scholar] [CrossRef] [PubMed]
19. Su, L.L.; Li, P.; Cheng, X.; Ding, X.Y.; Hao, M.; Lu, T.L.; Mao, C.Q.; Zhang, J. Effect of vinegar-processed Schisandra chinensis on bile metabolism in alcoholicliver iniury rats based on UPLC-Q/TOF-MS. *Chin. Tradit. Herb. Drugs* **2017**, *48*, 114–120. [Google Scholar]
20. Deng, X.Y.; Wu, H.F.; Li, Y.B.; Zhang, F.L.; Hu, Q.C.; Chen, Y.; Zhang, W.W.; Ma, X. Mechanism of paeonilforin on ameliorating a-naphthylisothiocyanate-induced cholestasis based on bile acid metabolomics. *Chin. Tradit. Herb. Drugs* **2024**, *55*, 148–158. [Google Scholar]
21. Fei, C.H.; Ji, D.; Tong, H.J.; Li, Y.; Su, L.L.; Qin, Y.W.; Bian, Z.H.; Zhang, W.; Mao, C.Q.; Li, L.; et al. Therapeutic mechanism of Salisb. rhizome against coronary heart disease based on integrated network pharmacology, pharmacological evaluation and lipidomics. *Front. Pharmacol.* **2022**, *13*, 950749. [Google Scholar] [CrossRef] [PubMed]
22. Hao, M.; Ji, D.; Li, L.; Su, L.L.; Gu, W.; Gu, L.Y.; Wang, Q.H.; Lu, T.L.; Mao, C.Q. Mechanism of Rhizoma on Acute Blood Stasis in Rats Based on a UPLC-Q/TOF-MS Metabolomics and Network Approach. *Molecules* **2019**, *24*, 82. [Google Scholar] [CrossRef] [PubMed]
23. Li, Y.; Li, M.; Mao, J.; Guo, Q.; Zhu, W.; Fu, R.; Wan, X.; Dong, W.; Li, L.; Mao, C.; et al. The processing mechanism of vinegar-processed Curcumae Rhizome enhances anti hepatic fibrotic effects through regulation of PI3K/Akt/mTOR signaling pathway. *Phytomedicine* **2024**, *135*, 156098. [Google Scholar] [CrossRef] [PubMed]
24. Mariotti, V.; Strazzabosco, M.; Fabris, L.; Calvisi, D.F. Animal models of biliary injury and altered bile acid metabolism. *Biochim. Biophys. Acta-Mol. Basis Dis.* **2018**, *1864*, 1254–1261. [Google Scholar] [CrossRef] [PubMed]
25. Tian, C.W.; Zhang, T.J.; Wang, L.L.; Shan, Q.; Jiang, L.H. The hepatoprotective effect and chemical constituents of total iridoids and xanthones extracted from Franch. *J. Ethnopharmacol.* **2014**, *154*, 259–266. [Google Scholar] [CrossRef] [PubMed]
26. Beuers, U.; Boberg, K.M.; Chapman, R.W.; Chazouilléres, O.; Invernizzi, P.; Jones, D.E.J.; Lammert, F.; Parès, A.; Trauner, M.; Liver, E.A.S. EASL Clinical Practice Guidelines: Management of cholestatic liver diseases. *J. Hepatol.* **2009**, *51*, 237–267. [Google Scholar] [CrossRef] [PubMed]
27. Chen, Y.; Hu, Q.; Zhang, W.; Gong, Q.; Yan, J.; Wang, Z.; Zhou, Z.; Ma, X.; Li, Y.; Lu, X.; et al. Chidan Tuihuang granule modulates gut microbiota to influence NOD1/RIPK2 pathway in cholestatic liver injury recovery. *Phytomedicine* **2024**, *135*, 156164. [Google Scholar] [CrossRef] [PubMed]
28. Feng, S.; Tang, J.; Wei, X.; Lu, Z.; Xu, Y.; Zhang, T.; Han, H. Swertia cincta and its main active ingredients regulate the PPAR-α pathway in anti-cholestatic liver injury. *J. Ethnopharmacol.* **2025**, *337*, 118956. [Google Scholar] [CrossRef] [PubMed]
29. Nasehi, Z.; Kheiripour, N.; Taheri, M.A.; Ardjmand, A.; Jozi, F.; Shahaboddin, M.E. Efficiency of Hesperidin against Liver Fibrosis Induced by Bile Duct Ligation in Rats. *Biomed. Res. Int.* **2023**, *2023*, 5444301. [Google Scholar] [CrossRef] [PubMed]
30. Sutton, H.; Karpen, S.J.; Kamath, B.M. Pediatric Cholestatic Diseases: Common and Unique Pathogenic Mechanisms. *Annu. Rev. Pathol.* **2024**, *19*, 319–344. [Google Scholar] [CrossRef] [PubMed]
31. Zhuang, T.; Wang, X.; Wang, Z.; Gu, L.; Yue, D.; Wang, Z.; Li, X.; Yang, L.; Huang, W.; Ding, L. Biological functions and pharmacological behaviors of bile acids in metabolic diseases. *J. Adv. Res.* **2024**, *75*, 779–792. [Google Scholar] [CrossRef] [PubMed]
32. Russell, D.W. The enzymes, regulation, and genetics of bile acid synthesis. *Annu. Rev. Biochem.* **2003**, *72*, 137–174. [Google Scholar] [CrossRef] [PubMed]
33. Marin, J.J.G.; Macias, R.I.R.; Briz, O.; Banales, J.M.; Monte, M.J. Bile Acids in Physiology, Pathology and Pharmacology. *Curr. Drug Metab.* **2016**, *17*, 4–29. [Google Scholar] [CrossRef] [PubMed]
34. Ma, Y.; Yang, H.; Wang, X.; Huang, Y.; Li, Y.; Pan, G. Bile acids as signaling molecules in inflammatory bowel disease: Implications for treatment strategies. *J. Ethnopharmacol.* **2025**, *337*, 118968. [Google Scholar] [CrossRef] [PubMed]
35. Hofmann, A.F.; Hagey, L.R. Bile acids: Chemistry, pathochemistry, biology, pathobiology, and therapeutics. *Cell. Mol. Life Sci.* **2008**, *65*, 2461–2483. [Google Scholar] [CrossRef] [PubMed]
36. Wagner, M.; Zollner, G.; Trauner, M. New molecular insights into the mechanisms of cholestasis. *J. Hepatol.* **2009**, *51*, 565–580. [Google Scholar] [CrossRef] [PubMed]

37. Kim, K.H.; Choi, J.M.; Li, F.; Dong, B.N.; Wooton-Kee, C.R.; Arizpe, A.; Anakk, S.; Jung, S.Y.; Hartig, S.M.; Moore, D.D. Constitutive Androstane Receptor Differentially Regulates Bile Acid Homeostasis in Mouse Models of Intrahepatic Cholestasis. *Hepatol. Commun.* **2019**, *3*, 147–159. [Google Scholar] [CrossRef] [PubMed]
38. Molinaro, A.; Marschall, H.U. Bile acid metabolism and FXR-mediated effects in human cholestatic liver disorders. *Biochem. Soc. Trans.* **2022**, *50*, 361–373. [Google Scholar] [CrossRef] [PubMed]
39. Brouwer, K.; Jackson, J.; Freeman, K.; Claire, R.S. Prediction of Cholestatic Hepatotoxicity: Integration of Transporter Inhibition and Interference with the FXR Mediated Adaptive Response to Bile Acids. *Hepatology* **2017**, *66*, 424a. [Google Scholar]
40. Guo, H.L.; Hassan, H.M.; Zhang, Y.; Dong, S.Z.; Ding, P.P.; Wang, T.; Sun, L.X.; Zhang, L.Y.; Jiang, Z.Z. Pyrazinamide Induced Rat Cholestatic Liver Injury through Inhibition of FXR Regulatory Effect on Bile Acid Synthesis and Transport. *Toxicol. Sci.* **2016**, *152*, 417–428. [Google Scholar] [CrossRef] [PubMed]
41. Wagner, M.; Fickert, P.; Zollner, G.; Fuchsbichler, A.; Silbert, D.; Tsybrovskyy, O.; Gonzalez, F.J.; Zatloukal, K.; Marschall, H.U.; Denk, H.; et al. Role of nuclear bile acid receptor, FXR, in determining ATP-binding cassette (ABC) transporter expression and cholestatic liver injury in common bile duct-ligated mice. *Gastroenterology* **2003**, *124*, A697–A698. [Google Scholar] [CrossRef]
42. Xu, G.R.; Salen, G.; Pan, L.X.; Forman, B.; Ananthanarayanan, M.; Erickson, S.K.; Shneider, B.; Shefer, S. Effect of the hydrophobic bile acid pool on hepatic FXR activation and regulation of CYP7A1. *Gastroenterology* **2002**, *122*, A24–A25. [Google Scholar]
43. Fuchs, C.D.; Simbrunner, B.; Baumgartner, M.; Campbell, C.; Reiberger, T.; Trauner, M. Bile acid metabolism and signalling in liver disease. *J. Hepatol.* **2024**, *82*, 134–153. [Google Scholar] [CrossRef] [PubMed]
44. Zollner, G.; Fickert, P.; Zenz, R.; Fuchsbichler, A.; Stumptner, C.; Kenner, L.; Ferenci, P.; Stauber, R.E.; Krejs, G.J.; Denk, H.; et al. Hepatobiliary transporter expression in percutaneous liver biopsies of patients with cholestatic liver diseases. *Hepatology* **2001**, *33*, 633–646. [Google Scholar] [CrossRef] [PubMed]
45. Natarajan, B.; Swaby, I.; Suchy, F.J.; Ananthanarayanan, M. Rat Bile salt export pump (Bsep) promoter: Isolation, characterization and evidence for trans-activation by Farnesoid acid receptor/Retinoid acid receptor (FXR/RXR). *FASEB J.* **2001**, *15*, A762. [Google Scholar]
46. Miszczuk, G.S.; Barosso, I.R.; Larocca, M.C.; Marrone, J.; Marinelli, R.A.; Boaglio, A.C.; Pozzi, E.J.S.; Roma, M.G.; Crocenzi, F.A. Mechanisms of canalicular transporter endocytosis in the cholestatic rat liver. *Biochim. Biophys. Acta-Mol. Basis Dis.* **2018**, *1864*, 1072–1085. [Google Scholar] [CrossRef] [PubMed]
47. Chen, H.; Huang, X.T.; Min, J.B.; Li, W.R.; Zhang, R.; Zhao, W.; Liu, C.H.; Yi, L.; Mi, S.Q.; Wang, N.S.; et al. Geniposidic acid protected against ANIT-induced hepatotoxity and acute intrahepatic cholestasis, due to Fxr-mediated regulation of Bsep and Mrp2. *J. Ethnopharmacol.* **2016**, *179*, 197–207. [Google Scholar] [CrossRef] [PubMed]

Disclaimer/Publisher's Note: The statements, opinions and data contained in all publications are solely those of the individual author(s) and contributor(s) and not of MDPI and/or the editor(s). MDPI and/or the editor(s) disclaim responsibility for any injury to people or property resulting from any ideas, methods, instructions or products referred to in the content.